Asociación Argentina
de Mecánica Computacional

Mecánica Computacional Vol XXV, pp. 263-280
Alberto Cardona, Norberto Nigro, Victorio Sonzogni, Mario Storti. (Eds.)
Santa Fe, Argentina, Noviembre 2006

ON THE EFFECTS OF PERTURBED CHANNEL FLOW ON THERMAL FIELD

Hugo D. Pasinato[a], **and Kyle D. Squires**[b]

[a]*Computational Transport Phenomena Group, Unidad A. Confluencia, Universidad Tecnológica Nacional, Plaza Huincul, hpasinato@uacf.utn.edu.ar,*

[b]*MAE Department, Arizona State University, Tempe, Arizona 85287-6106, squires@asu.edu*

Keywords: Velocity Temperature Dissimilarity, Direct Numerical Simulation.

Abstract. The direct numerical simulation of a fully developed turbulent flow with heat transfer and the direct numerical simulation of a perturbed turbulent channel flow with heat transfer, has been performed. Buoyancy effects were neglected, thus the temperature was considered as a passive scalar. For the first calculation, for non-perturbed flow, the isoflux, constant temperature, and uniform energy source boundary conditions has been used for the thermal field. Mean and turbulence values of velocity and temperature fields are compared with data from the literature for the isoflux case. The second calculation for the perturbed channel flow simulation with heat transfer, has been performed to investigate velocity and temperature fields dissimilarity. For this second calculation the uniform energy source case for the thermal field was used. Perturbations were applied into the flow locally by blowing from a span-wise slot at the lower wall, and suction from a similar slot at the upper wall. In this first work on perturbed turbulent channel flow, no developing calculation was used, rather than very small values of the transpiration velocity and slot width has been used in conjunction with a long periodic computational domain. The main results from this study show that the skin-friction and the Stanton number suffer clear changes owing to local blowing or suction. While local blowing yields a decreases of the skin-friction and the Stanton number, local suction increases these coefficients. Qualitatively the effects on both coefficients are similar for every perturbation. The local extremes, however, for the skin-friction are smaller than those for St. And also the region of velocity field affected by the perturbation is larger than for the temperature field. The budgets for the axial mean velocity and for the mean temperature show that the main source of dissimilarity for blowing is the mean pressure gradient and the convection terms. Mean pressure gradient make mean velocity to change in the wall region in a slight smoother way than mean temperature. This small differences in the variation of mean velocity and temperature yields dissimilarities in the turbulence production in the budget of the second moment of the fluctuations of axial velocity and temperature. The perturbed mean flow transfers energy to turbulence spreading out its effect into a larger region than those affected in the thermal field. The responsible for these differences in the mean flow and mean thermal field is the non-local effect of the mean pressure gradient on convection terms of the mean momentum equation. For the fluctuations of axial velocity and temperature fields the main causes of dissimilarity are the small differences in the behavior of the gradient of the mean values, which yields dissimilarity mainly in the turbulence production term.

1 INTRODUCTION

Turbulent heat transfer is a phenomenon of fundamental interest and technological relevance to a range of mechanical, aerospace, and chemical engineering processes in addition to a range of applications encountered in physics, biological and environmental sciences. Nevertheless, heat transfer predictions for most applications in practice utilize simplistic approaches based on Reynolds analogy, which implies similarity between momentum and heat transfer. This approach is computationally efficient since heat transfer predictions are essentially obtained from the turbulent velocity field at relatively little additional computational cost. However, most flows encountered in practice are far from equilibrium, the direct analogy between momentum and heat transfer fails, and use of the Reynolds analogy for predicting turbulent heat transfer can be very inaccurate (Spalart and Strelets, 2000; Kong, Choi, and Lee, 2001; Inaoka, Yamamoto, and Suzuki, 1999). Previous works show that there is a clear need to examine in detail the dissimilarities between heat and momentum transfer and to develop new approaches to predicting turbulent heat transfer in wall-bounded flows.

Since some time ago velocity and temperature fields dissimilarity in turbulent flows has been studied experimentally for different situations (Fulachier and Dumas, 1976; Antonia, 1980; Subramanian and Antonia, 1981; and Antonia, Krishnamoorthy and Fulachier, 1988). More recently, and as a consequence of the advance of large scale computers, a number of direct numerical simulations, DNS, have been performed addressing different aspects of heat transfer in turbulent flows. The first works computing a turbulent flow with heat transfer using DNS has been for developed thermal field (Kim and Moin, 1989; Kasagi, Tomita and Kuroda, 1992; Kasagi and Ohtsubo, 1993; Kawamura, Abe, and Matsuo, 1999; Na, Papavasiliou, and Hanratty, 1999; Zhou, Cui, and Zhang, 2002). In one of these works Kim and Moin (1989) studied the scalar transport in a developed turbulent channel flow for different boundary conditions for the temperature field, presenting results for the isoflux case or constant wall heat case. In another work, Kasagi, Tomita, and Kuroda (1992) have done an extensive and well documented DNS of a developed turbulent channel flow with heat transfer using also the isoflux case. And more recently Prandtl, Pr, and Reynolds, R_τ, numbers effects in turbulent heat transfer has been addressed in developed turbulent flow. Kawamur, Abe and Matsuo(1999) used DNS of a fully turbulent channel flow with the objective to study the Pr and R_τ effects on the turbulent Prandtl number, Pr_t. They found that near the wall the Pr_t is approximately 1.0, and independently of Re_τ and Pr, if $Pr > 0.2$. They show that the effect of Pr on Pr_t is more important for lower values of Pr. In another work Na, Papavassiliou, and Hanratty (1999) used DNS in order to study the effect of Pr on temperature field, in a turbulent channel flow. As boundary conditions they used a heated lower wall and a coled upper one. They studied the effect of Pr in the range $0.3 - 10.0$ using an Euler approach, and in the range $0.1 - 2400$ with a Lagrangian formulation. They found that for $Pr > 1$ and for $y^+ > 5$, the influence of Pr on the eddy diffusivity is quite small. On the other hand, however, large effects were found of Pr on the velocity and temperature correlation fields, temperature and temperature variance. They suggest that the $\nu_\theta = \nu_t$ assumption, which means $Pr_t = 1.0$, is a good approximation for the buffer region, outside the viscous layer, and for the logarithmic region only. In contrast, for the core region $\nu_\theta > \nu_t$, or $Pr_t < 1.0$. All these results for developed turbulent channel flow.

More recently, dissimilarity between velocity and temperature fields has been addressed numerical and experimentally in disturbed, or non-equilibrium, turbulent flows (Suzuki, Suzuki, and Sato (1988); Inaoka, Yamamoto, and Suzuki, 1999; Kong, Choi and Lee, 2001). Non-equilibrium turbulent flow means a turbulent flow where the equilibrium between turbulence

production and dissipation, that nominally exists in the wall region, has been disrupted by some kind of perturbation. These perturbations can consist of, for example, wall blowing or suction, transverse pressure gradient, stream-wise curvature, wall roughness, wall temperature variations, or with the insertion of an obstacle into a boundary layer. In one of his work Suzuki, Suzuki, and Sato (1988) studied the skin friction and heat transfer coefficient differences with the insertion of a cylinder into a boundary layer, and found that hot outward and cold wallward interactions were intensified more strongly than were sweeps and ejections of momentum in this kind of perturbation. Also, they found that near the wall the sweep/ejection process modification contribute negatively to momentum transfer, and that hot outward/cold wallward phenomena were more intense that momentum sweep/ejection. Then, based on this previous work, Inaoka, Yamamoto, and Suzuki (1999) addressed numerical and experimentally the influence of the von Karman vortex street behind a square road in a boundary layer. And they found that while a reduction of the skin friction downstream of the inserted cylinder was measured, there was on the other hand a significant enhancement of heat transfer. They have given the explanation that suppression of the von Karman vortex reduces significantly the heat transfer behind the road, thus decreasing the momentum/heat transfer dissimilarity. And the main reason for this phenomena is a decouple between u' and v' in the Reynolds stress $\langle u'v' \rangle$, in contrast to the thermal stress $\langle v'\theta' \rangle$ in turbulent heat transfer. Also Kong, Choi and Lee (2001) have addressed the velocity and temperature fields dissimilarity in a perturbed turbulent boundary layer using DNS. The perturbation was provided into the boundary layer by local blowing or local suction from a spanwise slot. They found that the skin friction and the Stanton number were significantly changed due to blowing and suction. Above the slot they found that the main source of dissimilarity was the mean pressure gradient. Whereas downstream of the slot the source of dissimilarity was mainly due to the velocity-pressure gradient second moment.

In the present work results from the DNS of a developed turbulent flow with heat transfer and the DNS of a perturbed turbulent channel flow with heat transfer are presented. In both calculations the temperature was considered as a passive scalar. For the first calculation, with non-perturbed flow, the isoflux, constant temperature, and uniform energy source boundary conditions has been used, however mean and turbulence values of velocity and temperature fields only for the isoflux case are presented. The second calculation with heat transfer has been performed addressing the velocity and temperature fields dissimilarity, using the uniform energy source case as boundary condition. Perturbations are applied into the flow by local blowing from a span-wise slot at the lower wall, and local suction from a similar slot at the upper wall. In this first work on perturbed turbulent channel flow with heat transfer presented by the authors, no inflow-outflow boundary conditions were used for the channel flow. Rather than a very small values for the transpiration dimensionless velocity of $v^+ = 0.20$, and very small dimensionless spanwise slot width $W^+ = 60$, were used in conjunction with a long periodic computational domain equal to 7π. The following is a detail of the sections in this work. In §2 the numerical procedure is presented for the case of fully developed turbulent channel flow with heat transfer in first term, and then for the perturbed case with heat transfer. Then in §3, in a first subsection, mean values for velocity, temperature, and turbulence values, for the fully developed turbulent channel are shown and compared with similar data from the literature. Then in a second subsection, results and discussion for the perturbed turbulent channel flow with heat transfer are presented. And finally in §5 the main conclusions are commented.

2 NUMERICAL PROCEDURE

In this section a description of the numerical aspects of the simulations, first for the fully developed turbulent channel flow, and second for the perturbed turbulent channel flow are presented. In this paper, u, v, and w are the instantaneous velocities in the streamwise (x), wall-normal (y), and spanwise (z) directions, respectively. All instantaneous variables are decomposed in a mean value and a fluctuation; e.g. $u = U + u'$.

2.1 Developed Turbulent Channel Flow

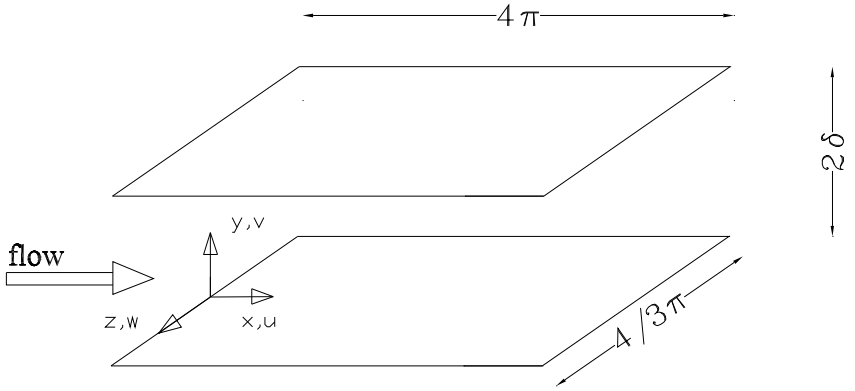

Figure 1: Computational domain for fully developed turbulent channel flow.

The computational domain for the DNS of the fully developed turbulent flow and the coordinate system are shown in Figure 1. Then, the governing equations in dimensionless form are the continuity, the unsteady Navier-Stokes and the energy equations for incompressible flow and heat transfer

$$\frac{\partial u_i}{\partial x_j} = 0 \tag{1}$$

$$\frac{\partial u_i}{\partial t} + \frac{\partial}{\partial x_j} u_j u_i \;=\; \frac{1}{R_\tau} \frac{\partial^2}{\partial x_j \partial x_j} u_i \;-\; \frac{\partial p}{\partial x_i} \tag{2}$$

$$\frac{\partial \theta}{\partial t} + \frac{\partial}{\partial x_j} u_j \theta \;=\; \frac{1}{Pr R_\tau} \frac{\partial^2}{\partial x_j \partial x_j} \theta \;+\; S_e \tag{3}$$

where the nondimensionalization was done using the friction velocity v_τ and half channel distance between walls δ, and the friction temperature $T_\tau = q_w / \rho \; c_p \; u_\tau$. Where θ is the dimensionless temperature, which has a different nondimensionalization for every thermal case as it is explained below, q_w is the heat flux at the wall, and c_p and ρ are the constant pressure specific heat coefficient and the density, respectively. In these equation Pr, and R_τ are the molecular Prandtl and turbulent Reynolds numbers, respectively, and S_e is a dimensionless energy source term, which is different for every thermal case as it is explained below.

The computational domain for the fully developed turbulent flow was chosen to be 4π and $4\pi/3$ (1885, and 628 in wall units) in x and z directions, respectively. The size of the computational domain in x and z-directions was checked using two-point velocity correlation. This

computational domain is discretized with a $128 \times 128 \times 128$ grid, which in wall units means $\Delta x^+ = 14.72$, $\Delta y^+ = 0.09 - 6.72$, and $\Delta z^+ = 4.90$, in the three directions respectively. In comparison, the Kim and Moin's (1989) and Kasagi, Tomita, and Kuroda's (1992) discretization used in their spectral resolutions are respectively $\Delta x^+ = 17.7$, $\Delta y^+ = 0.05 - 4.4$, $\Delta z^+ = 5.9$, and $\Delta x^+ = 18.4$, $\Delta y^+ = 0.08 - 4.9$, $\Delta z^+ = 7.4$. And, using also a spectral code Kim, Moin and Moser (1987) used $\Delta x^+ = 12$, and $\Delta z^+ = 7$, using a 192x129x160 grid. The time step was $0.0008\delta/u_\tau$ or $0.12\nu/u_\tau^2$.

The unsteady Navier-Stokes equations were solved numerically at a Reynolds number R_τ equal to 150, based on the v_τ wall friction velocity and half channel distance between walls δ. The DNS code used in the present work for the velocity fields was developed by Prof. Kyle Squires' group at ASU. In this code the incompressible momentum equation are discretized by the second-order accurate central-difference scheme. The Poisson equation for the pressure field is Fourier-transformed with respect to the streamwise and spanwise periodic directions and the resulting three-diagonal equations are solved directly for each time step. The flow field is advanced in time using a fractional-step method, with the Adams-Bashforth scheme for the time discretization. For the thermal field a numerical code has been presently developed, in which the spatial derivatives of the diffusion term are approximated using the same discretization of the flow field, while the convection terms are approximated using the QUICK scheme (Leonard, 1979). The time advance for temperature, on the other hand, is done with the same scheme used for the flow field.

For the velocity field periodic boundary conditions are used in the spanwise and in the streamwise direction, and non-slip boundary conditions at both walls. As initial condition, an instantaneous velocity field of a developed turbulent flow was supplied from a previous calculation for a turbulent channel flow with the same DNS code.

After the velocity field is calculated at each time step, the temperature field was obtained integrating the energy equation. The working fluid is air, with a Prandtl number $Pr = 0.71$. Any buoyancy effect was neglected, thus temperature was considered as a passive scalar. In x and z direction, as for velocity, periodic boundary condition were used for temperature, whereas at walls three cases with different boundary conditions were used. The constant heat flux or isoflux case, the constant wall temperature, and the uniform heat source cases were solved. The dimensionless temperature, θ, and the energy source term in the energy equation, S_e, are different for every case. For constant wall heat flux, $\theta = (T_w - T)/T_\tau$, and $S_e = u_1/U_1$, thus $\theta = 0$ as boundary condition at walls. For the constant wall temperature case, with heat flux from the upper to the lower wall, $S_e = 0$, and the dimensional boundary conditions are $T_{LW} = (1 - \alpha)T_\tau$, $T_{UW} = (1 + \alpha)T_\tau$. Where LW and UW mean lower-wall and upper-wall, respectively, and α is some arbitrary absolute value less than 1. Thus dimensionless temperature, $\theta = (T - T_{LW})/T_\tau$, boundary conditions are $\theta_{LW} = 0$, and $\theta_{UW} = 2\alpha$. The uniform scalar source case solved in the present work is similar to case I solved in Kim and Moin (1989), who used a source term equal to $2/Re_\tau Pr$. In the present study, however, the source is a constant energy source uniformly distributed in the domain, equal to q_w/δ, which in dimensionless form is $S_e = 1.0$. The boundary condition at walls for this case is $\theta = 0$, as for the isoflux case. As initial conditions for the thermal field a mean temperature from the law of the wall, $\theta^+ = 2.785\ ln(y^+) + 2.09$, was given for the isoflux case. Then a fully developed thermal field from this last calculation is given for the scalar source and for the constant wall temperature cases. For the constant wall temperature, however, it should be done a transformation of this developed thermal field using the absolute value of the constant α.

Preliminary computations were conducted on a coarse grid $64 \times 128 \times 64$ and then the

flow and thermal fields were interpolated onto the $128 \times 128 \times 128$ grid. The time integration was repeated until the velocity(temperature) field was judged to be fully developed in the new simulation using the mean velocity (temperature), the Reynolds stresses (thermal stress) and the wall shear stress (wall heat flux). A time of about $1,000\nu/u_\tau^2$ was required to reach a stationary state, but in all cases time of $2,400\nu/u_\tau^2$ were running before the averaging process was taken. Then the statistics time integration was taken equal to $32\delta/u_\tau$, $40,000$ computational time step, or $3,600\nu/u_\tau^2$, in order to define mean values.

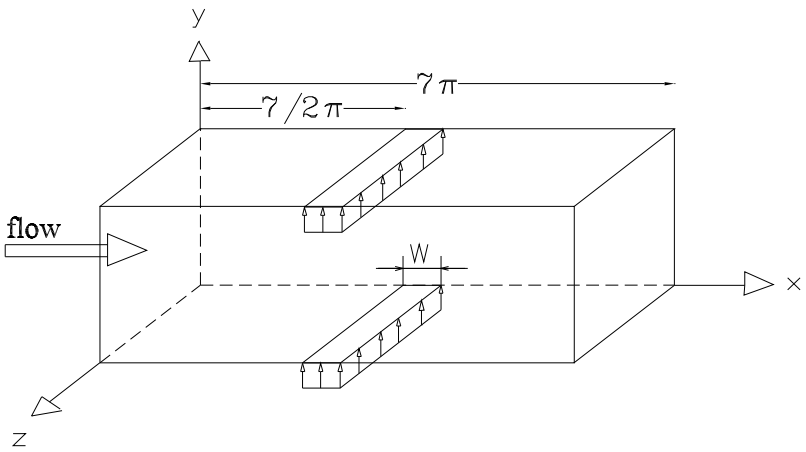

Figure 2: Computational domain for the perturbed turbulent channel flow.

2.2 Perturbed Turbulent Channel Flow

In the present work, the computational domain, Figure 2, for the perturbed case was similar to the non-perturbed case, with the exception of the L_x period of the channel in the axial direction. In this Figure W is the spanwise slot width used for local blowing or suction, which has its start point at the middle of the L_x axial period. The remain aspects of the numerical procedure are the same as for the fully developed turbulent channel flow. In the following, W^+ and v^+ are these values nondimensionalized with the wall variables, u_τ and ν. Blowing and suction were provided using a transpiration velocity as boundary condition for the normal wall velocity at the spanwise slots. The energy equation was solved for the uniform heat source case, for which the boundary condition are $\theta = 0$, and $S_e = 1$, as it is commented above.

As it is mentioned in the abstract, being these the first results presented by the authors for perturbed turbulent channel flow, no developing turbulent channel flow simulation was used. In other words, rather than to use an inflow-outflow DNS for the perturbed channel flow, with inflow boundary condition from a developed turbulent flow from a parallel calculation, a long computational domain with periodic boundary condition in the axial direction, in conjunction with very small value for the magnitude of the transpiration velocity and very small width for the spanwise slot with blowing or suction, was used. Next results on this ongoing work on velocity and temperature fields dissimilarity will be obtained using an inflow-outflow DNS, using a parallel DNS for developed turbulent channel flow in order to have fully developed inflow boundary conditions.

In the present work, however, different tests were done to define the axial dimension L_x, changing the magnitudes of transpiration velocity, and the slot width. These tests were done checking the mean velocity(temperature), the skin-friction(Stanton number) at both walls, and

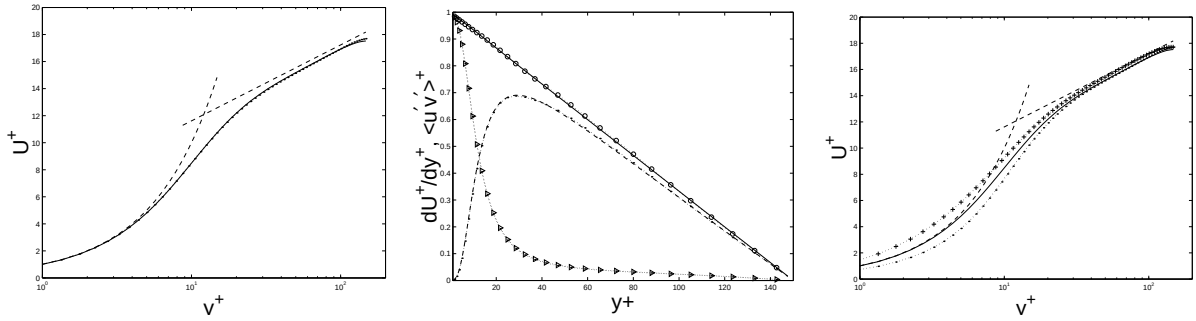

(a) (b) (c)

Figure 3: Comparison of mean values for fully developed and perturbed turbulent channel flow. (a)Distribution of mean velocity. Solid line, fully developed; $\cdots\cdots$, perturbed 1000 wall units upstream of slot. (b)Distribution of dimensionless total, viscous and Reynolds stresses. Fully developed flow: solid line, total; $- - - - -$, $\langle u'v' \rangle$; $\cdots\cdots$, viscous. Perturbed flow 1000 wall units upstream of slot.$\circ \cdot \circ \cdot \circ \cdot \circ$, total; $\cdots\cdots$, $\langle u'v' \rangle$; $\triangleright \cdot \triangleright \cdot \triangleright \cdot \triangleright$, viscous. (c)Comparison of mean velocity above the slots with fully developed flow: Solid line, fully developed flow; $\cdots\cdots$, above the slot with blowing; $+ \cdot + \cdot + \cdot +$, above the slot with suction.

the Reynolds(thermal) stresses at a point 1000 wall units upstream of the slot. And the computational domain finally chosen was $L_x = 7\pi$, with $v^+ = 0.20$ for the dimensionless transpiration velocity and $W^+ = 60$ for the dimensionless spanwise slot. These values yields differences in the mean values(first order and second order moments) almost imperceptible, as it is shown in Figures 3(a) -3(b), which show mean values of velocity and Reynolds stress 1000 wall units upstream of the spanwise slot. It can be seen in Figure 3(a) for the mean velocity only slight differences in the core of the channel. The Reynolds stress at the same point upstream in Figure 3(b) presents no differences with the fully developed flow. On the other hand, Figure 3(c) shows the distribution of the mean velocity for the fully developed turbulent channel flow in comparison with the distribution above the blowing slot and above the suction slot. In this Figure it is clear that above the slots perturbations affect basically the mean flow only in the buffer region. The velocity through the logarithmic sub-region presents, on the other hand, a minor effect due to suction, and a slight effect due to blowing.

3 RESULTS AND DISCUSSION

3.1 Results for Fully Developed Turbulent Channel Flow

The mean and turbulence values for the fully developed channel flow are presented in this subsection. Mean values here means Reynolds averaged mean value in the $x - z$ plane. Kasagi, Tomita, and Kuroda's (1992), and Kim, Moin, and Moser's (1987) results for Re_τ equal to 150 and 180, respectively, are used for comparison. The resultant Reynolds number for the present calculation based on the mean velocity and 2δ is 4552, which is in good agreement with Kasagi et al.'s (1992) calculation bulk Reynolds equal to 4580. The dimensionless mean and turbulence values for the velocity and temperature fields are shown in Figures 4(a) -6(c) as a function of $y^+ = yu_\tau/\nu$. The agreement of the mean velocity with Kim at al.'s (1987), and Kasagi at al.'s (1992) values, and the law of the wall in Figure 4(a) is good with a very small under

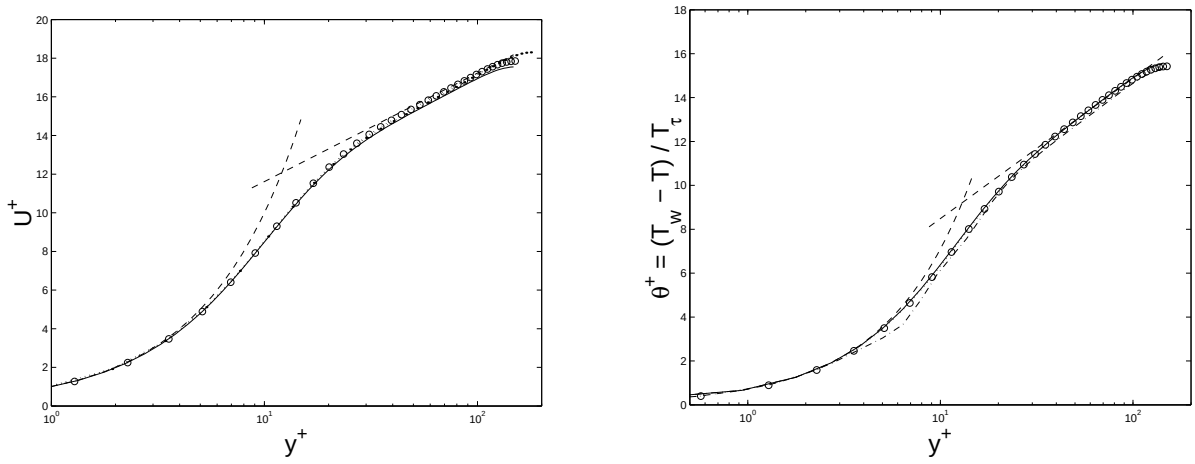

(a) (b)

Figure 4: (a)Distribution of dimensionless mean velocity for fully developed turbulent channel flow. Solid line, present calculation, $Re_\tau = 150$; $\circ \cdot \circ \cdot \circ \cdot \circ$, Kasagi, Tomita, and Kuroda (1992), $Re_\tau = 150$; $\cdots\cdots$, Moser, Kim, and Mansour (1999), $Re_\tau = 180$; $- - - - -$, law of the wall $U^+ = ln(y^+)/0.41 + 6.0$,and $U^+ = y^+$. (b)Distribution of dimensionless mean temperature for fully developed turbulent channel flow for the isoflux case. Solid line, present calculation, $Re_\tau = 150$, $Pr = 0.71$; $\circ \cdot \circ \cdot \circ \cdot \circ$, Kasagi, Tomita, and Kuroda (1992), $Re_\tau = 150$, $Pr = 0.71$; $\cdot - \cdot - \cdot - \cdot$, Kader (1981); $- - - - -$, $\theta^+ = 2.78\ ln(y^+) + 2.09$, and $\theta^+ = Pr\ y^+$.

prediction of the mean velocity in the core region of the channel. Temperature mean values for the developed thermal field are shown in Figures 4(b) for the isoflux case, in comparison with Kasagi et al's (1992) results, the law of the wall, $\theta^+ = 2.78\ ln(y^+) + 2.09$, and Kader's (1981) empirical polynomials. As it is shown in Figure 4(b) the agreement of the mean temperature is excellent.

Reynolds stresses and thermal Reynolds stresses are shown in Figures 5(a)-5(b). The agreement of Reynolds stresses is good. As regarding thermal Reynolds stresses and for the fully developed channel flow for the isoflux case, the wall-normal heat flux balance can be deduced from the Reynolds averaged energy equation as

$$\frac{1}{Pr}\frac{\partial \theta^+}{\partial y^+} \; - \; \langle u'^+ \theta'^+ \rangle = \{1 \; - \; \frac{\int_0^{y^+} U^+ \, dy^+}{\int_0^{Re_\tau} U^+ \, dy^+}\} \tag{4}$$

where U^+ is the dimensionless Reynolds averaged mean axial velocity.

In equation (4) on the left-hand side, the first term is the molecular heat flux, and the second one is the turbulent heat flux. The term on the right-hand side is the Reynolds averaged source term for the isoflux case. All these terms are shown in Figure 5(b). In this Figure it is shown that the thermal Reynolds stresses of the present work show a good agreement with Kasagi et al's (1992) results, although there is a very slight over predictions of the turbulent flux $\langle v'\theta' \rangle$ approximately at $y^+ = 30$.

Figures 6(a) show the root-mean-square, rms, of the fluctuations of velocity, u'^+, v'^+, and w'^+. These results present a slight under predictions in comparison with Kasagi et al.'s (1992) results. From $y^+ = 20$ to the center of the channel the rms present a small under prediction with maximum values less than 3%, mainly for the fluctuation of the axial velocity. These dif-

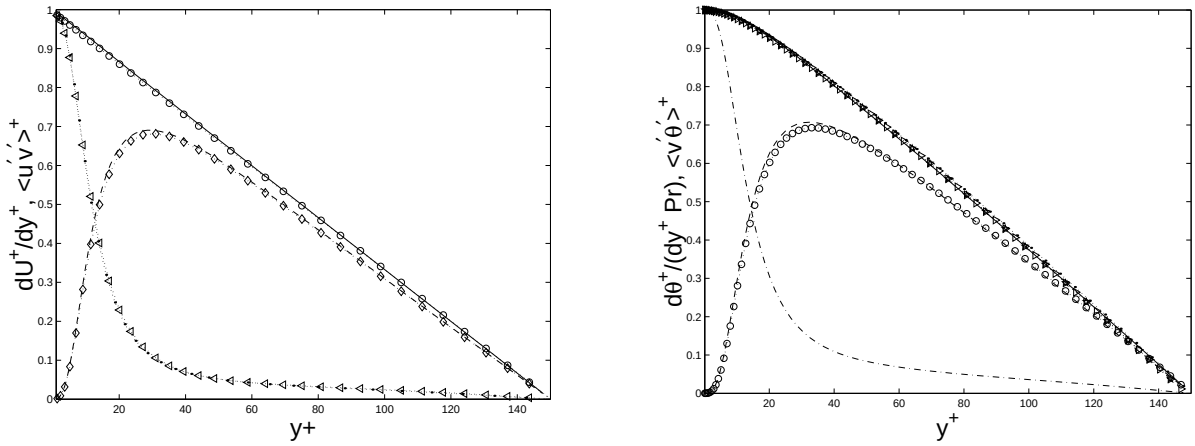

(a) (b)

Figure 5: (a) Distribution of dimensionless total, viscous and Reynolds stresses for fully developed turbulent channel flow. Present calculation, $Re_\tau = 150$. Solid line, total; $- - - - -$, $\langle u'v' \rangle$; $\cdots\cdots$, viscous. Kasagi, Tomita, and Kuroda (1992), $Re_\tau = 150$. $\circ\cdot\circ\cdot\circ\cdot\circ$, total; $\diamond\cdot\diamond\cdot\diamond\cdot\diamond$, $\langle u'v' \rangle$; $\triangleleft\cdot\triangleleft\cdot\triangleleft\cdot\triangleleft$, viscous. (b)Distribution of dimensionless molecular, Reynolds and total thermal stresses, for fully developed turbulent channel flow for the isoflux case. Present calculation $Re_\tau = 150$, $Pr = 0.71$; solid line, total stresses; $\cdot - \cdot - \cdot - \cdot$, molecular; $- - - - -$, $\langle v'\theta' \rangle$; $\cdots\cdots$, rhs of Equation(4). Kasagi, Tomita, and Kuroda (1992), $Re_\tau = 150$, $Pr = 0.71$. $\triangleright\cdot\triangleright\cdot\triangleright\cdot\triangleright$, total thermal stress; $\circ\cdot\circ\cdot\circ\cdot\circ$, $\langle v'\theta' \rangle$; $*\cdot*\cdot*\cdot*$, rhs of Equation(4).

ferences are attributed to the better precision for very high-frequency components of turbulent fluctuations, of the spectral codes used by Kasagi et al. (1992) in their calculation in comparison with the second-order central differences used in the present work. Then Figures 6(b) - 6(c) show the rms of the thermal fluctuations θ'^+ and the heat fluxes $\langle u'\theta' \rangle^+$, and $\langle v'\theta' \rangle^+$. In these Figures there is an under prediction of the present results of approximately 9% at the maximum value of the turbulent heat flux $\langle u'\theta' \rangle$, and in the order of 5% for the rms of the fluctuations of temperature. As regarding these differences, however, it is worth to mention that Kasagi et al.'s (1992) results for the turbulent heat flux $\langle u'\theta' \rangle^+$, and for the rms of fluctuation of temperature, present an over predicted in comparison with Kim and Moin's (1989) results of approximately 5%, which are not presented here (Figure 4, and 5, in Kasagi, Tomita, and Kuroda, 1992).

3.2 Results for Perturbed Turbulent Channel Flow

In this section the mean and turbulence values for the perturbed velocity and temperature fields are presented. Mean values in this subsection means Reynolds averaged in the spanwise direction, z, and the results presented are for the transpiration velocity $v^+ = 0.20$, and slot width $W^+ = 60$, both in wall units. The energy equation, on the other hand, is solved for the uniform heat source case, as it is commented above, which means that the dimensionless source term $S_e = 1$. Thus, for fully developed flow, the solutions of the axial momentum and energy equations differ only in the diffusion term owing to the Pr, which value is 0.71. Thus for a fully developed turbulent channel flow the similarity between axial momentum and energy is almost complete, and this is the base flow which is perturbed by blowing or suction. Although both results for blowing and suction are presented, for space reason discussion is focused on blowing

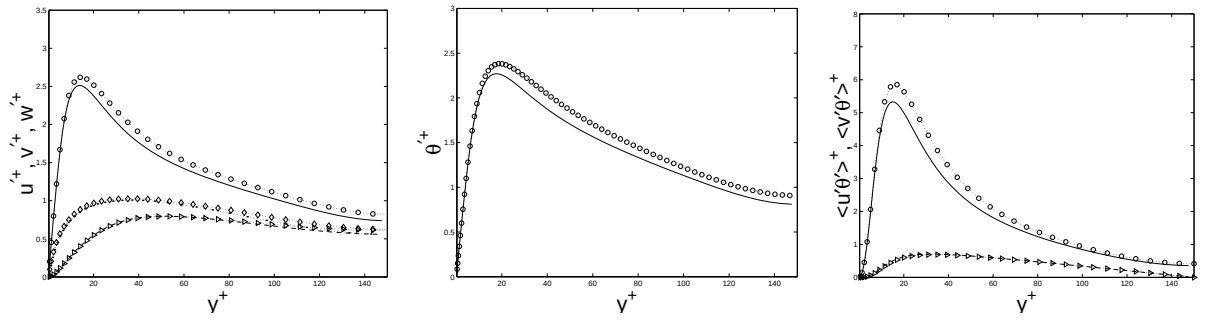

(a) (b) (c)

Figure 6: (a)Distribution of dimensionless rms of velocity fluctuations for the fully developed turbulent channel flow. Present calculation, $Re_\tau = 150$. Solid line, u'^+; $- - - - -$, v'^+; $\cdots\cdots$, w'^+. Kasagi, Tomita, and Kuroda (1992), $Re_\tau = 150$. $\circ\cdot\circ\cdot\circ\cdot\circ$, u'^+; $\diamond\cdot\diamond\cdot\diamond\cdot\diamond$, v'^+; $\triangleright\cdot\triangleright\cdot\triangleright\cdot\triangleright$, w'^+.(b)Distribution of dimensionless rms of temperature fluctuations for fully developed turbulent channel flow for the isoflux case. Solid line, present calculation; $\circ\cdot\circ\cdot\circ\cdot\circ$, Kasagi, Tomita, and Kuroda (1992). (c)Distribution of dimensionless axial and wall normal turbulent heat flux for fully developed turbulent channel flow for the isoflux case. Present calculation, solid line, $\langle u'\theta'\rangle$; $\cdot - \cdot - \cdot - \cdot$, $\langle v'\theta'\rangle$. Kasagi, Tomita, and Kuroda (1992), $\circ\cdot\circ\cdot\circ\cdot\circ$, $\langle u'\theta'\rangle$; $\cdot - \cdot - \cdot - \cdot$, $\langle v'\theta'\rangle$.

effects in the present work.

(a)Skin-Friction and Stanton Number: Figures 7(a) shows the axial distribution of half the time-averaged skin-friction, $f/2 = \tau_w/(\rho\bar{U}^2)$, and the time-averaged Stanton number, $St = h/\rho c_p\bar{U})$, for blowing and suction, normalized for its values for fully developed flow. Where τ_w is the wall shear stress, ρ, the density, $\bar{U}$ the axial mean velocity in the whole domain, $h = q_w/(T_b - T_w)$ is the convective heat transfer coefficient, and T_b is the bulk temperature.

The skin-friction and the Stanton number suffer clear local changes due to blowing or suction. While local blowing yields a decreases of the skin-friction and the Stanton number, local suction increases these coefficients, although the local changes for blowing are smaller than those for suction. There are however small dissimilarities between the skin-friction and the St. The changes in St are abrupt, with its starting point almost coincident with the location of the upstream border of the spanwise slot. On the other hand, the local maximum and minimum for the skin-friction are smaller than the respectively values for the St. But the most important difference is the smoother variation of the skin-friction, which means a smoother change of the mean velocity in contrast with mean temperature. As it is shown below, this slight difference in both mean fields is a source of dissimilarity in the turbulence production terms of velocity and temperature fluctuation fields. And the primary reason for this dissimilarity is the mean axial pressure gradient term, whose distribution is shown in Figure 7(b). The axial pressure gradient is shown at the walls $y^+ = 0$, and at the beginning of the logarithmic region, $y^+ = 30$. For blowing the pressure gradient term at the wall presents a local maximum at approximately 30 wall units upstream of the slot border, a local minimum above the slot, and a second local maximum at 90 wall units downstream of the upstream slot border. In contrast, for suction there is two local minimums, and a maximum value above the slot, in almost the same locations. Thus, it can be said that blowing causes qualitatively the opposite effect of suction on the axial pressure gradient term. The slight differences are the absolute magnitudes of these extreme values.

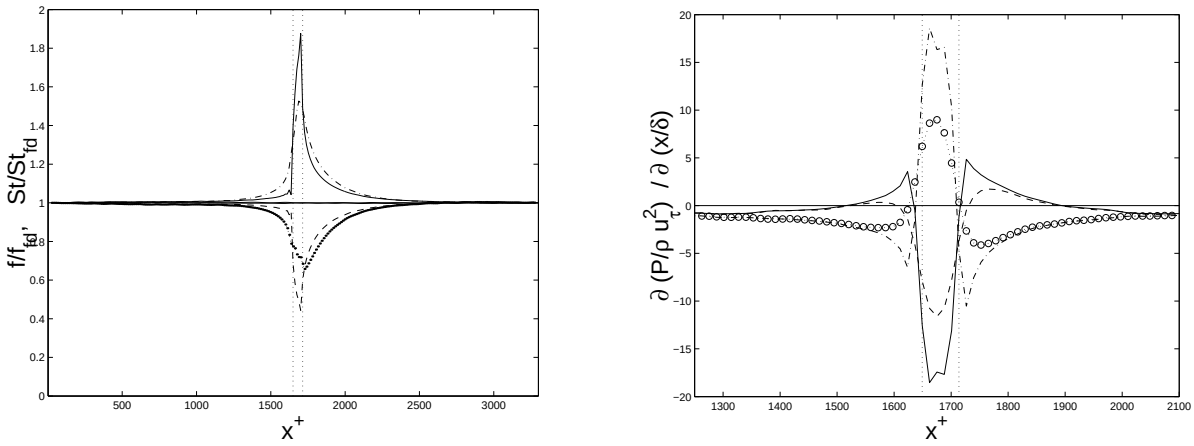

(a) (b)

Figure 7: (a)Streamwise variations of the normalized skin friction and Stanton number due to blowing and suction for $v^+ = 0.20$, and $W^+ = 60$. Skin-friction: $\cdots\cdots$, blowing; $\cdot - \cdot - \cdot - \cdot$, suction. Stanton number: solid line, suction; $- - - - -$, blowing. Dotted lines denote the spanwise slot location. (b)Streamwise distribution of the dimensionless axial pressure gradient due to blowing and suction, for $v^+ = 0.20$, $W^+ = 60$. Blowing: Solid line, $y^+ = 0$; $- - - - -$, $y^+ = 30$. Suction: $\cdot - \cdot - \cdot - \cdot$, $y^+ = 0$; $\circ \cdot \circ \cdot \circ \cdot \circ$, $y^+ = 30$. Dotted lines denote the location of the spanwise slot.

(b)Budget for the Mean Streamwise Velocity and Temperature Fields: Figures 8-9 show the budgets for the mean streamwise velocity and temperature fields, equations (5-6), for the fully developed channel flow, and for perturbed flow with parameters $v^+ = 0.20$ and $W^+ = 60$ at the locations of the three extreme values of the mean axial pressure gradient term at the wall, as shown in Figure 7(b). In equations (5-6), the first term on the right-hand side is the convection term, the second is the turbulent transport, the third is the source term for momentum(mean axial pressure gradient) or heat,S_e, respectively, and the last term is the diffusion term.

$$\frac{\partial U}{\partial t} = -\{U\frac{\partial U}{\partial x} + V\frac{\partial U}{\partial y}\} - \{\frac{\partial \langle u'u' \rangle}{\partial x} + \frac{\partial \langle u'v' \rangle}{\partial y}\} - \frac{\partial P}{\partial x} \; + \; \{\frac{1}{R_\tau}\frac{\partial^2 U}{\partial x \partial x}\} \tag{5}$$

$$\frac{\partial \theta}{\partial t} = -\{U\frac{\partial \theta}{\partial x} + V\frac{\partial \theta}{\partial y}\} - \{\frac{\partial \langle u'\theta' \rangle}{\partial x} + \frac{\partial \langle v'\theta' \rangle}{\partial y}\} + \; S_e \; + \; \{\frac{1}{PrR_\tau}\frac{\partial^2 \theta}{\partial x \partial x}\} \tag{6}$$

Figures 8 shows that a local blowing yields a perturbation in the convection terms of the axial momentum equation, which is balanced mainly by the pressure gradient term. These are the two terms that suffer the most important changes in the mean axial momentum budget through the blowing region. In contrast, the diffusion and turbulent transport terms do not suffer significantly due to blowing. For the energy budget, however, the convective and diffusion terms suffer the most important changes and are almost balanced by each other. The turbulent transport term in both budgets do not suffer any significant modification in comparison with fully developed turbulent channel flow.

Therefore the main source of dissimilarity in the budget for the mean values U and θ, are the main axial pressure gradient, and the convection, for the first variable, and the convection and diffusion terms for the second one. Since changes in the mean temperature are abrupt the diffusion term takes an important rule in the budget of the mean temperature. Thus, heat is

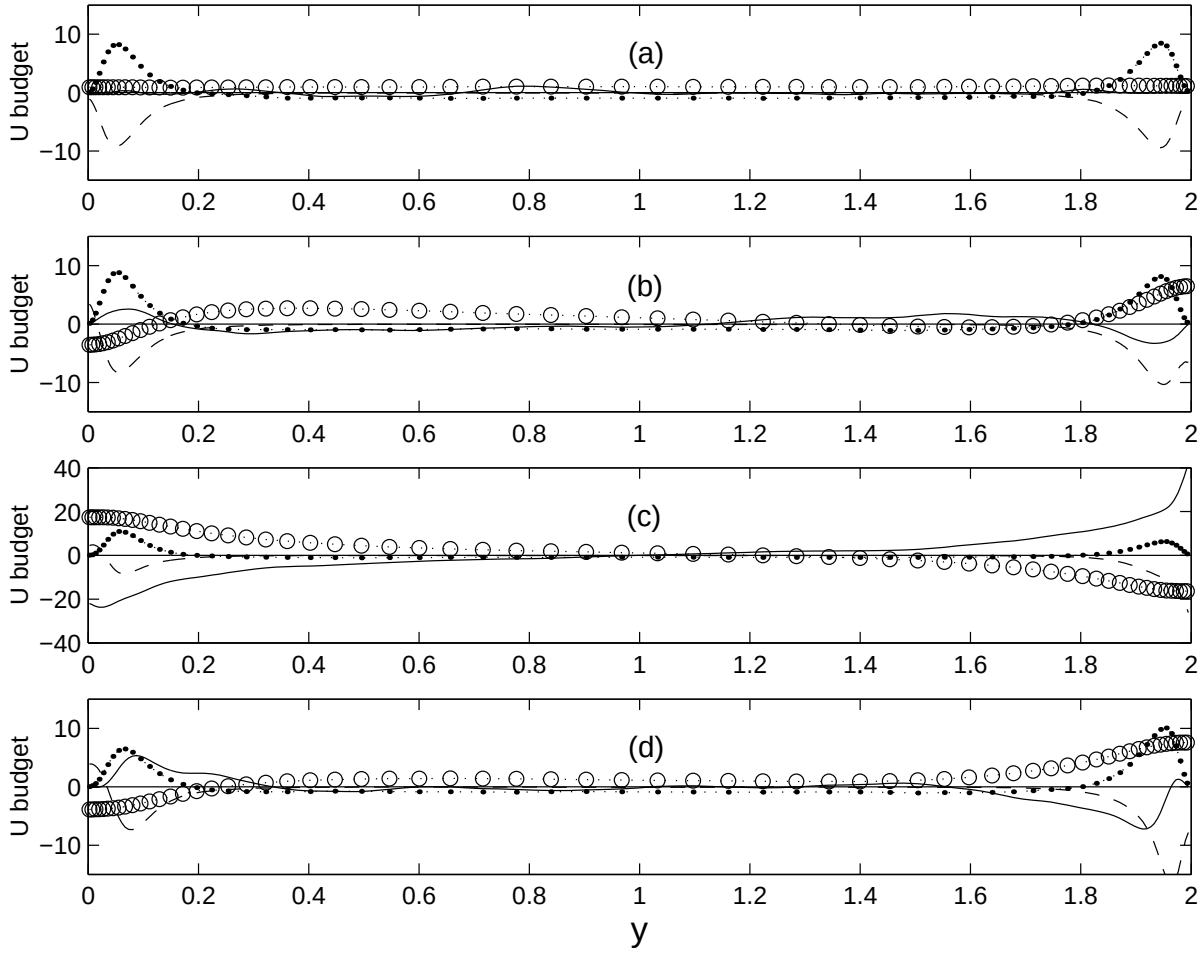

Figure 8: Mean streamwise-velocity budget normalized by u_τ^2/δ for (a) non-perturbed flow, and for low wall blowing(y=0) and upper wall suction(y=2) for $v^+ = 0.20$ $W^+ = 60$ at three location: (b)35 wall unit upstream of the slot;(c) 38 downstream; (d)90 downstream of the slot beginning. Solid line, convection term; $- - - - -$, diffusion term; $\cdots\cdots$, turbulent transport term; $\circ \cdot \circ \cdot \circ \cdot \circ$, pressure gradient term.

transfered by convection and diffusion in order to adjust in the blowing region. In contrast in the momentum budget the transference of momentum is basically due to convection, if pressure gradient is thought as a convection potential. Therefore the main dissimilarity between mean velocity and temperature fields are the higher gradient of the temperature field, and the source for this difference is the main pressure gradient in the momentum budget, as it was expected.

(c)Budget of the Second Moment of Axial Velocity and Temperature Fluctuations: Figures 10-11 show the budgets for the second moment of the fluctuations of the streamwise velocity $\langle u'u' \rangle$, and temperature $\langle \theta'\theta' \rangle$, equations (7-8). The budgets are shown for the fully developed turbulent channel flow, and for blowing and suction with parameters $v^+ = 0.20$, $W^+ = 60$. In equations (7-8), the first term on the right-hand side is the convection term, the second is the diffusion term, the third is the turbulent transport, the fourth is the turbulent production, the fifth term is the turbulence dissipation, and the sixth term, which is only in equation (7), is the velocity-pressure gradient term.

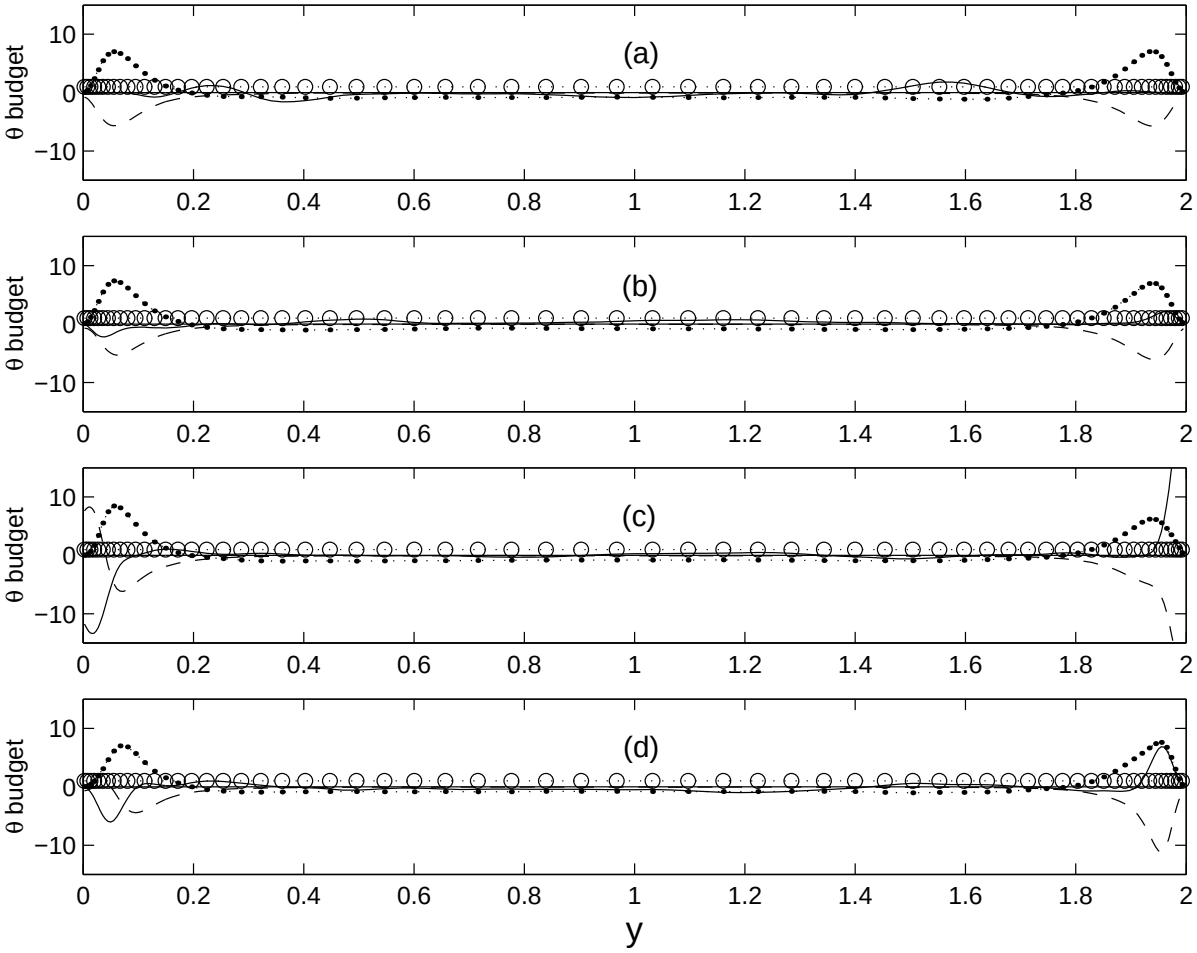

Figure 9: Mean temperature budget normalized by $\theta_\tau u_\tau/\delta$ for (a) non-perturbed flow, and for low wall blowing(y=0) and upper wall suction(y=2) for $v^+ = 0.20$ $W^+ = 60$ case at three location: (b)35 wall unit upstream of the slot beginning;(c) 38 downstream; (d)90 downstream. Solid line, convection term; $- - - - -$, thermal diffusion term; $\cdots\cdots$, thermal turbulent transport term; $\circ\cdot\circ\cdot\circ\cdot\circ$, source term.

$$\frac{\partial\langle u'u'\rangle}{\partial t} = -\{U_j\frac{\partial\langle u'u'\rangle}{\partial x_j}\} + \{\frac{1}{R_\tau}\frac{\partial^2\langle u'u'\rangle}{\partial x_j\partial x_j}\} - \{\frac{\partial\langle u'u'u'_j\rangle}{\partial x_j}\}$$
$$-\{2\langle u'u'_j\rangle\frac{\partial U}{\partial x_j}\} - \{\frac{2}{R_\tau}\langle\frac{\partial u'}{\partial x_j}\frac{\partial u'}{\partial x_j}\rangle\}$$
$$-\{2\langle u'\frac{\partial p'}{\partial x}\rangle\} \tag{7}$$

$$\frac{\partial\langle\theta'\theta'\rangle}{\partial t} = -\{U_j\frac{\partial\langle\theta'\theta'\rangle}{\partial x_j}\} + \{\frac{1}{PrR_\tau}\frac{\partial^2\langle\theta'\theta'\rangle}{\partial x_j\partial x_j}\} - \{\frac{\partial\langle\theta'\theta'u'_j\rangle}{\partial x_j}\}$$
$$-\{2\langle\theta'u'_j\rangle\frac{\partial\theta}{\partial x_j}\} - \{\frac{2}{PrR_\tau}\langle\frac{\partial\theta'}{\partial x_j}\frac{\partial\theta'}{\partial x_j}\rangle\} \tag{8}$$

As it is known, in equations (7-8) the first, second, and third terms on the right-hand side are transport terms; transport by convection, by diffusion, and by turbulent velocity(temperature) fluctuations. All these terms redistribute turbulent kinetic energy and thermal energy, in both

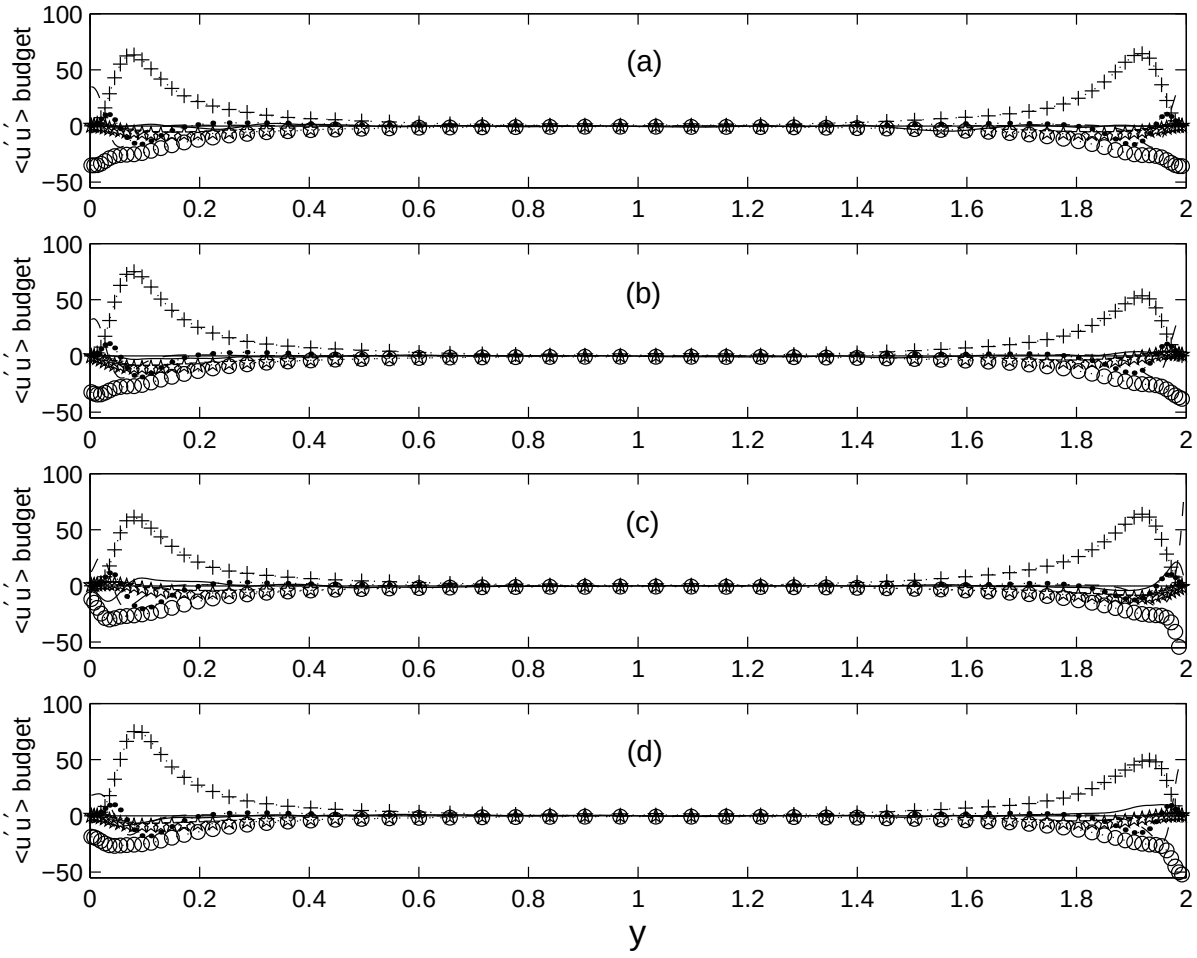

Figure 10: $\langle u'u' \rangle$ budget normalized by u_τ^3/δ for (a) non-perturbed flow, and for low wall blowing(y=0) and upper wall suction(y=2) for $v^+ = 0.20$ $W^+ = 60$ at three location: (b)35 wall unit upstream of the slot beginning;(c) 38 downstream; (d)90 downstream. Solid line, convection term; $- - - - -$, diffusion term; $+ \cdot + \cdot + \cdot +$, turbulent production term; $\cdots\cdots$, turbulent transport term; $\circ \cdot \circ \cdot \circ \cdot \circ$, dissipation term; $* \cdot * \cdot * \cdot *$, velocity-pressure gradient term.

budgets respectively, from one point in the flow to another. The sixth term, which is only in equations (7), can be written as $\langle \partial u' p'/\partial x \rangle - \langle p' \partial u'/\partial x \rangle$, representing a redistribution of energy in space, the first part, and a redistribution of energy among different velocity components, the second part. Thus, only the fourth and fifth terms on the second line of these equations are responsible for the production and dissipation of turbulence in both fields.

Therefore looking first at the production of turbulence in $\langle u'u' \rangle$ and $\langle \theta'\theta' \rangle$ budgets, in Figures 10-11, the first noteable dissimilarity between both fields is the locations where the production terms present differences in comparison with the production term for fully developed flow. For the blowing region the production term of $\langle u'u' \rangle$ is greater in Figures 10-b, d, and smaller than the developed flow value, in Figures 10-c. In contrast, the production term of $\langle \theta'\theta' \rangle$, is greater in Figure 10-c, and smaller than the developed flow value, in Figures 10-b and d. It is important to mention that, based on results not presented here, these differences are more clear for higher magnitude of the transpiration velocity. Therefore this seems to be the most remarkable source of dissimilarity.

The follow try to be an explanation for this phenomenon. The turbulence production in

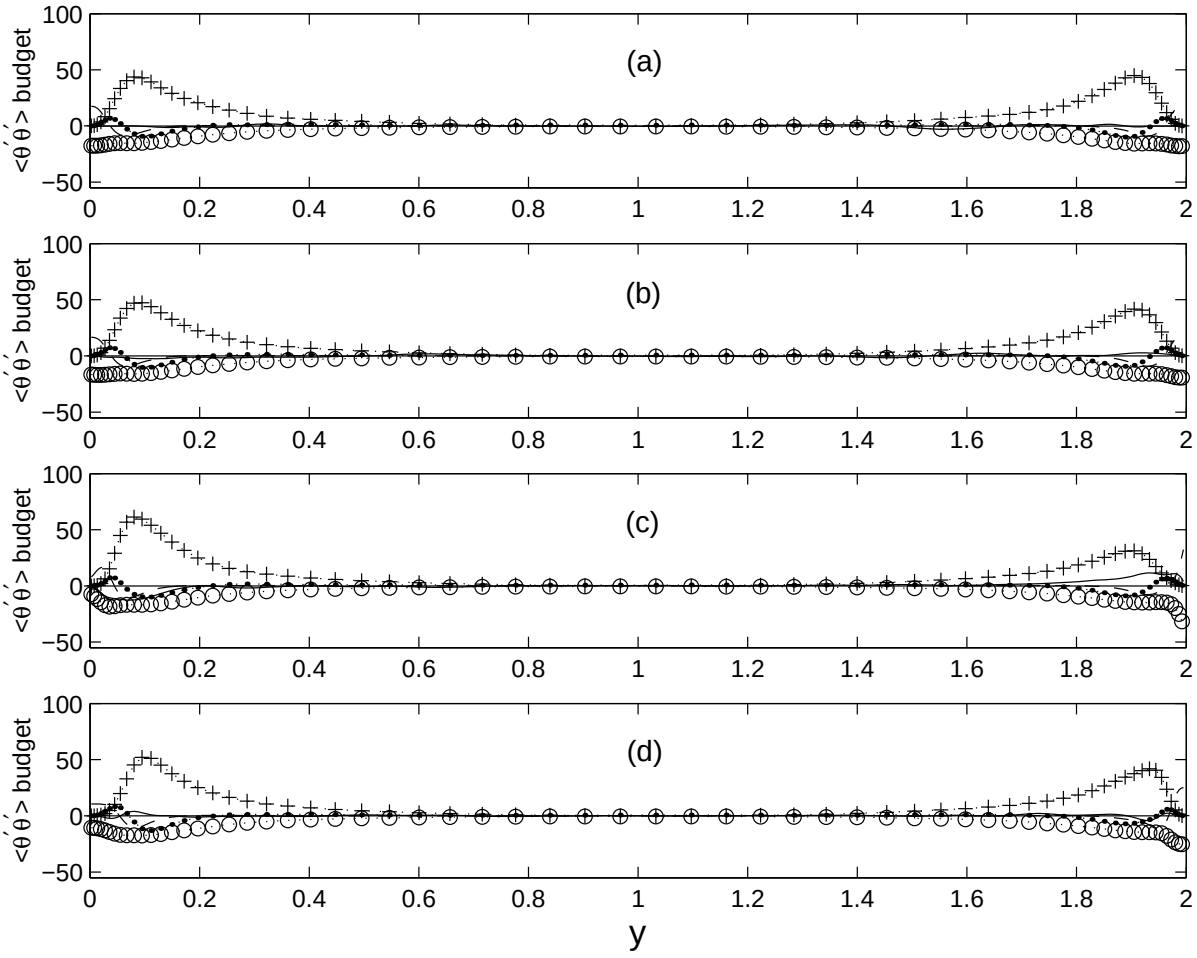

Figure 11: $\langle\theta'\theta'\rangle$ budget normalized by $T_\tau^2 u_\tau/\delta$ for (a) non-perturbed flow, and for low wall blowing(y=0) and upper wall suction(y=2) for $v^+ = 0.20$ $W^+ = 60$ at three location: (b)35 wall unit upstream of the slot beginning;(c) 38 downstream; (d)90 downstream. Solid line, convection term; $- - - - -$, diffusion term; $+ \cdot + \cdot + \cdot +$, turbulent production term; $\cdots\cdots$, turbulent transport term; $\circ \cdot \circ \cdot \circ \cdot \circ$, dissipation term.

$\langle u'u'\rangle$ receives contribution from the terms $-\{2\langle u'v'\rangle \partial U/\partial y\}$, and $-\{2\langle u'u'\rangle \partial U/\partial x\}$, while for $\langle\theta'\theta'\rangle$ receive from $-\{2\langle\theta'v'\rangle \partial\theta/\partial y\}$, and $-\{2\langle\theta'u'\rangle \partial\theta/\partial x\}$. And it can be shown (by results not shown here) that in both budgets the production associated with the wall normal gradient of the mean values is one order of magnitude larger than those associated with the axial gradient of mean values. Which is a known result for fully developed turbulent flow, and it continues to be valid here for small perturbations. Thus, the major contribution to turbulence production is coming from the term with wall normal gradient in both budgets. The major dissimilarity, however, in both budgets is coming from the minor contribution of the production term associated with the axial gradient of the mean values.

In other words, the basic turbulent production in both budget is coming from the term with wall-normal gradient, but the dissimilarity is coming from the minor contribution of the axial gradient. And the reason for this is that U changes occur basically upstream and downstream of the spanwise slot, Figure 7(a). While changes in θ are abrupt and basically above the slot.

Therefore, the axial gradient of U with its minor contribution upstream and downstream of the slot yields two maximum values of turbulent production at these locations. In contrast, the

axial gradient of θ, which change abruptly above the slot, yields a turbulence minor contribution that produces a maximum of turbulence production above the slot, as it is seen in Figures 11-c. With different words it can say that the maximum of turbulence production in both budgets have different location and the responsible for this phenomenon is the axial gradient of the mean velocity and temperature fields. It is worth to remember here, also, that the differences in the axial behavior of the mean values U and θ is the mean pressure gradient term in the U budget.

As it is known, the production term in the velocity field apparently serves to exchange kinetic energy between the mean flow and turbulence. The same is true for the temperature field. But while in thermal field the gradient are abrupt and the production is concentrated above the slot, for the velocity field the change are smoother owing to the pressure gradient term. Thus in the velocity field the energy coming from the mean flow is spread out in space in a larger region than in the temperature field. And the causes for this dissimilarity are the small differences of the wall normal and axial gradients of the mean fields U and θ.

The term that balances the turbulence production in the $\langle u'u' \rangle$ budget is mainly dissipation, but the terms that more contribute to dissimilarity are convection and the velocity-pressure gradient terms. The velocity-pressure gradient term is not in the temperature field, and convection is essentially different in both fields. On the other hand, in $\langle \theta'\theta' \rangle$ budget, turbulent production is mainly balanced also by dissipation. In spite of the importance of the dissipation, turbulent transport, and diffusion terms, they have qualitatively the same behavior in both budgets, and do not contribute significantely to dissimilarity.

Thus, in conclusion, it can be said that the main source of dissimilarity between the two second moment budgets for the blowing zone are the turbulent production term, the velocity-pressure gradient term, and the convection term. And the source of all these differences have clearly its origin in the non-local transfer effect of mean pressure gradient, as it was expected, on the other hand. It is important to remark here that much of the information of this dissimilarity is in the gradient of the mean values, U and θ. And also that the dissimilarity occurs basically owing to terms with minor contribution in both fields.

4 CONCLUSIONS

The DNS of a fully developed turbulent flow with heat transfer and the DNS of a perturbed turbulent channel flow with heat transfer, has been presented in this work. These calculations have been performed for $Re_\tau = 150$, and $Pr = 0.71$. Any buoyancy effect was neglected, thus the temperature was considered as a passive scalar in both calculations.

For the first calculation, the isoflux, constant temperature, and uniform energy source as boundary condition has been used. Mean and turbulence values of velocity and temperature fields were compared with data from the literature for the isoflux case.

The second calculation for the perturbed channel flow simulation with heat transfer, has been performed to investigate velocity and temperature fields dissimilarity. The boundary condition for the thermal problem was the uniform heat source. Perturbations were applied into the flow by local blowing from a span-wise slot at the lower wall, and local suction from a similar slot at the upper wall. Very small values of the transpiration velocity and slot width has been used, in conjunction with a long period of the computational domain, in order to have at some degree developed turbulent flow upstream of the span-wise slots. The main results from this study show that the skin-friction and the Stanton number suffer clear changes owing to local blowing or suction. While local blowing yields a decreases of the skin-friction and the

Stanton number, local suction increases these coefficients. The local extremes of these two coefficients,however, are different. The Stanton number presents always higher extreme values. The main source of dissimilarity, on the other hand, for blowing in the wall region, for the mean velocity and temperature budgets, is the pressure gradient and the convection terms. While for the turbulence of the axial velocity and temperature the dissimilarity are mainly owing to the turbulent production term. Although with smaller contribution, also the velocity-pressure gradient term, and the convection term increase the dissimilarity. These dissimilarities have clearly its origin in the non-local transfer effect of the mean pressure gradient, as it was expected, on the other hand. The mean pressure gradient yields a smoother of the perturbed mean velocity field in comparison with those of the mean temperature. Although the main source of turbulence production of the axial velocity and temperature is the wall-normal gradient of the mean fields, small differences between the axial gradients yield the most important dissimilarity between the turbulence fields of velocity and temperature. In other words, in spite of its minor contribution to the production of turbulence, the axial gradient of the mean fields is the most important secondary source of dissimilarity.

Thus, it can say that the mean pressure gradient, as expected, is the primary source of dissimilarity, and that the higher values of the gradient of the thermal field is the secondary source of dissimilarity between the velocity and temparature fields.

REFERENCES

[1] R.A. Antonia. Behavior of the turbulent Prandtl number near the wall. *Int. J. Heat Mass Transfer*, **23**, 906-908, 1980.

[2] R.A. Antonia, L.V. Krishnamoorthy, and L. Fulachier. Correlation between the longitudinal velocity fluctuation and temperature fluctuation in the near-wall region of a turbulent boundary layer. *Int. J. Heat Mass Transfer*, **31**(4), 723-730, 1987.

[3] Y.M. Chung and H.J. Sung. Initial Relaxation of Spatially Evolving Turbulent Channel with Blowing and Suction. *AIAA J.*, **39**(11), 2091-2099, 2001.

[4] L. Fulachier and R. Dumas. Spectral analogy between temperature and velocity fluctuations in a turbulent boundary layer. *J. Fluid Mechanics*, **77**, 257-277, 1976.

[5] J. Inaoka, J. Yamamoto, and K. Suzuki. Dissimilarity between heat transfer and momentum transfer in a disturbed turbulent boundary layer with insertion of a rod - modeling and numerical simulation. *Int. J. Heat Fluid Flow*, **20**, 290-301, 1999.

[6] B.A. Kader. Temperature and Concentration Profiles in Fully Turbulent Boundary Layers. *Int. J. Heat Mass Transfer*, **24**(9), 1541-1544, 1981.

[7] K. Kasagi Y. Tomita, and A. Kuroda. Direct numerical simulation of the passive scalar field in a turbulent channel flow. *Transaction of ASME, Journal of Heat Transfer*, **114**, 598-606, 1992.

[8] N. Kasagi and Y. Ohtsubo. Direct numerical simulation of low Prandtl number thermal field in a turbulent channel flow. In *Turbulent Shear Flow*, **8**, 97-119, 1993.

[9] H. Kawamura, H. Abe, and Y. Matsuo. DNS of turbulent heat transfer in channel flow with respect to Reynolds and Prandtl number effects. *Int. J. Heat Fluid Flow*, **20**, 196-207, 1999.

[10] J. Kim, P. Moin and R. Moser. Turbulent statistics in fully developed channel flow at low Reynolds number. *J. Fluid Mechanics*, **177**, 133-166, 1987.

[11] J. Kim, and P. Moin. Transport of Passive Scalar in a Turbulent Channel Flow. In *Turbulent Shear Flow*, **6**, 86-96. 1989.

[12] H. Kong, H. Choi, and J.S. Lee.Dissimilarity between the velocity and temperature fields in a perturbed turbulent thermal boundary layer. *Physics of Fluids*, **13**(5), 1466-1479, 2001.

[13] B.P. Leonard .A stable and accurate convective modeling procedure based on quadratic upstream interpolation. *Comp. Method Appl. Mech. Eng.*, **19**, 59, 1979.

[14] . Na, D.V. Papavasiliou, and T. J. Hanratty. Use of direct numerical simulation to study the effect of Prandtl number on temperature fields. *Int. J. Heta and FLuid Flow*, **20**, 187-195, 1999.

[15] P.R. Spalart and M.K. Strelets. Mechanisms of transition and heat transfer in a separation bubble, *Journal of Fluid Mechanics*. **403**, 329-349, 2000.

[16] C.S. Subramanian and R.A. Antonia. Effect of Reynolds number on a slightly heated turbulent boundary layer. *Int. J. Heat Mass Transfer*, **24**(11), 1833-1846, 1981.

[17] . Suzuki, K. Suzuki, and T. Sato. Dissimilarity between heat and mass transfer in a turbulent boundary layer disturbed by a cylinder. *Int. J. Heat Mass Transfer*, **31**, (2), 259-265, 1988.

[18] H. Zhou, G. Cui, and Z. Zhang. Dependence of turbulent flux on molecular Prandtl number. *Physics of Fluids*, **14**(7), 2388-2394, 2002.